Understanding the discrete genetic toggle switch phenomena using a discrete 'nullcline' construct inspired by the Markov chain tree theorem

Andreas Petrides* and Glenn Vinnicombe*

***Abstract*— Nullclines provide a convenient way of characterising and understanding the behaviour of low dimensional nonlinear deterministic systems, but are, perhaps not unsurprisingly, a poor predictor of the behaviour of discrete state stochastic systems in the low numbers regime. Such models are appropriate in many biological systems. In this paper we propose a graphical discrete 'nullcline-like' construction, inspired by the Markov chain tree theorem, and investigate its application to the original genetic toggle switch, which is a feedback interconnection of two mutually repressing genes. When the feedback gain (the 'cooperativity') is sufficiently large, the deterministic system exhibits bistability, which shows itself as a bimodal stationary distribution in the discrete stochastic system for sufficiently large numbers. However, at small numbers a third mode appears corresponding to roughly equal numbers of each molecule. Without cooperativity, on the other hand (i.e. low feedback gain), the deterministic system has just one stable equilibrium. Nevertheless, the stochastic system can still exhibit bimodality. In this paper, we illustrate that the discrete 'nullclines' proposed can, *without the need to calculate the steady state distribution*, provide an efficient graphical way of predicting the shape of the stationary probability distribution in different parameter regimes, thus allowing for greater insights in the observed behaviours.**

I. Introduction

Since its first appearance in 2000 [7], the synthetic genetic toggle switch has inspired a lot of interest among both the biological as well as the engineering community, as it provides a potential explanation of how decisions are made in biological processes. Its design includes two competing proteins, x and y, each repressing (inhibiting) the transcription of the other. In (1) the standard symmetric birth and death reactions for the proteins (transcription factors) x and y are presented [15], [14], [18], [7], with the difference that their values are normalised by their respective equilibrium values, $\bar{x}$ and $\bar{y}$. The production of protein x is negatively regulated by protein y, through binding of m copies of y to the promoter of x (and vice versa).If m, the Hill coefficient, satisfies $m > 1$, then the transcription factors are said to exhibit cooperative binding, or simply 'cooperativity' [14], [3]. k is a constant, associated with the inverse of the repression strength [15], [14], [4].

The traditional analysis using Ordinary Differential Equations [7] predicts two stable steady states in the cooperative case ($m > 1$) and one stable steady state in the non-cooperative case ($m = 1$). However, experimental results and exact stochastic simulations [15] have shown that when the concentrations are small, then the system with cooperative binding can also exhibit trimodality, something that is not predicted using the Chemical Langevin Equation [9].

Furthermore, by the use of Langevin equations [4], direct use of the Chemical Master Equations [14] or exact stochastic simulations [14] as well as experimentally [23], it has been shown that the non-cooperative case can also exhibit bimodality in certain cases, without this being predicted in the deterministic analysis.

$$\begin{aligned} x &\xrightarrow{\frac{k^m \bar{x}}{k^m + \left(\frac{x}{\bar{y}}\right)^m}} x+1, x \xrightarrow{\beta x} x-1 \\ y &\xrightarrow{\frac{k^m \bar{y}}{k^m + \left(\frac{y}{\bar{x}}\right)^m}} y+1, y \xrightarrow{\beta y} y-1 \end{aligned} \tag{1}$$

In this paper, we develop heuristic tools that allow the analysis of such stochastic systems represented as a graph of microstates, and with minimal calculations. For the toggle switch, we aim to predict the behaviour of the system as the equilibrium size changes.

We begin by showing that, with our choice of normalised reaction rates, the Jacobian obtained about the equilibrium is invariant to the equilibrium size. This allows us to discriminate the stochastic effects resulting from the change of equilibrium number from any deterministic phenomena.

Secondly, without explicitly finding the steady state of the Chemical Master Equation, which represents the problem as a continuous time Markov Process, we look for a way of understanding the effect the change of equilibrium size has on the system through a novel graphical construction, proposing a discrete 'nullcline-like' analysis based simply on the transition rates (propensities) of the system. This graph construction is inspired by the well-known Markov chain tree theorem and its graph theoretic representation, which states that the stationary probability of a node in a strongly-connected graph, if regarded as a root, is proportional to the sum of the weights of its associated rooted directed spanning trees, also known as arborescences [2], with orientation from the leaves to the root. The weight of each directed spanning tree is defined as the product of the weights of the edges that form the tree.

Our aim, essentially, is to infer how the mean weight of the directed spanning trees rooted at a particular node compares with those rooted at the other nodes (as for all given roots the number of directed spanning trees is constant in balanced graphs [24]). Instead of looking at the problem directly, which would make it combinatorially very challenging, we try to extract as much information as

Research supported by the Engineering and Physical Sciences Research Council, Award ref. 1468514

*Department of Engineering, University of Cambridge, CB2 1PZ, Cambridge, UK ap650@cam.ac.uk, gv@eng.cam.ac.uk

we can from the requirements that must be satisfied for a subgraph to be a rooted directed spanning tree.
The requirements that a subgraph is a rooted directed spanning tree are that it is acyclic, the outdegree of the rooted vertex is equal to zero and the outdegree of each other vertex is equal to one [11].

Selecting a particular directed edge when forming the rooted directed spanning tree (arborescence) places a constraint on the rest of the directed edges that can be selected in order to satisfy the requirements that the directed subgraph created is a rooted directed spanning tree. In fact, it is this constraint that makes the related directed spanning tree problems much more combinatorially difficult than the corresponding undirected spanning tree problems, as for example is the classical problem of finding the spanning tree of minimum weight [6], [10], [12].
Heuristically, for consistently forming large weight arborescences (and therefore having a large mean weight of arborescences), the location of the root would be expected to allow the consistent selection of the most beneficial (i.e. the largest of the two) direction for each edge. Based on this argument, we suggest that knowing the preferential transition direction of each edge can be a useful tool that could enable inference of the final form of the stationary probability distribution.

In the 1-D Markov chain case (as well as in higher dimensions when detailed balance is observed) the 'net propensity' used to construct the discrete 'nullclines' fully define the stationary distribution. For the 2-D case without detailed balance, illustrated through the Genetic toggle switch example, it is shown that it can be a very useful heuristic tool, both in the symmetric as well as in the asymmetric cases.

II. The deterministic analysis provides an invariant to the equilibrium size Jacobian

In this section, we illustrate that the usual deterministic analysis, transforming the discrete problem into a continuous time stochastic differential equation, can provide an invariant Jacobian at equilibrium.

It is standard to approximate (1) as a pair of coupled SDE's:

$$\begin{aligned} dx &= \left(\frac{k^m\bar{x}}{k^m+\left(\frac{y}{\bar{y}}\right)^m}-\beta x\right)dt+\sqrt{\frac{k^m\bar{x}}{k^m+\left(\frac{y}{\bar{y}}\right)^m}+\beta x}\;dW_1 \\ dy &= \left(\frac{k^m\bar{y}}{k^m+\left(\frac{x}{\bar{x}}\right)^m}-\beta y\right)dt+\sqrt{\frac{k^m\bar{y}}{k^m+\left(\frac{x}{\bar{x}}\right)^m}+\beta y}\;dW_2 \end{aligned} \tag{2}$$

From Eq. 2, deterministic ODEs can be obtained by setting the noise terms to zero (taking the large numbers limit) [25]. This results in

$$\begin{aligned} \dot{x} &= \frac{k^m\bar{x}}{k^m+\left(\frac{y}{\bar{y}}\right)^m}-\beta x \\ \dot{y} &= \frac{k^m\bar{y}}{k^m+\left(\frac{x}{\bar{x}}\right)^m}-\beta y \end{aligned} \tag{3}$$

An equilibrium solution of the ODEs of (3), when $\frac{k^m}{k^m+1}=\beta$, is $(x,y)=(\bar{x},\bar{y})$. Linearising and then normalising about this point, letting $\delta x = x-\bar{x}$ and $\delta y = y-\bar{y}$ [22],

$$\begin{pmatrix} \frac{\dot{\delta x}}{\bar{x}} \\ \frac{\dot{\delta y}}{\bar{y}} \end{pmatrix} = \begin{pmatrix} -\beta & -\frac{\beta m}{k^m+1} \\ -\frac{\beta m}{k^m+1} & -\beta \end{pmatrix} \begin{pmatrix} \frac{\delta x}{\bar{x}} \\ \frac{\delta y}{\bar{y}} \end{pmatrix} \tag{4}$$

Thus the equilibrium Jacobian when there is no cooperativity ($m=1$) is invariant and given by

$$J = \begin{pmatrix} -\beta & -\frac{\beta}{k+1} \\ -\frac{\beta}{k+1} & -\beta \end{pmatrix} \tag{5}$$

III. Chemical Master Equation and its graph theoretic interpretation

A. Chemical Master Equation

To investigate the stochastic effects due to the change of equilibrium size (e.g. small number effects), it is possible to directly approximate the steady state of the Chemical Master Equation (CME) by truncating the infinite grid into a finite one [21], [17]. The microstate of the system involving, in this case, two species, x and y, is defined as $\mathbf{x(t)}=\{x(t),y(t))\} \in \mathbb{N}^2$.The discrete Chemical Master Equation is illustrated in (6), where the positive real transition rates, also called propensities, from one state to another (i.e. from state $\mathbf{x}'$ to state $\mathbf{x}$) are represented by $A(\mathbf{x},\mathbf{x}')$, while $P(\mathbf{x},t)$ is the continuous time probability of each discrete state [16].

$$\frac{dP(\mathbf{x},t)}{dt} = \sum_{\mathbf{x}'\neq\mathbf{x}} \Big[A(\mathbf{x},\mathbf{x}')P(\mathbf{x}',t)-A(\mathbf{x}',\mathbf{x})P(\mathbf{x},t)\Big] \tag{6}$$

The general Chemical Master Equation can be represented explicitly for this system, where we represent the microstate probability at time t, $P(\mathbf{x},t)$, using its x and y components, as $P_{x,y}$:

$$\begin{aligned} \tfrac{dP_{x,y}}{dt} &= \tfrac{k^m\bar{x}}{k^m+\left(\frac{y}{\bar{y}}\right)^m}P_{x-1,y}+\beta(x+1)P_{x+1,y} \\ &+\tfrac{k^m\bar{y}}{k^m+\left(\frac{x}{\bar{x}}\right)^m}P_{x,y-1}+\beta(y+1)P_{x,y+1}- \\ &\left(\tfrac{k^m\bar{x}}{k^m+\left(\frac{y}{\bar{y}}\right)^m}+\beta x+\tfrac{k^m\bar{y}}{k^m+\left(\frac{x}{\bar{x}}\right)^m}+\beta y\right)P_{x,y}, \\ \beta &= \tfrac{k^m}{1+k^m} \end{aligned} \tag{7}$$

The equation can also be written in matrix vector form, where $\mathbf{A}$ is called the matrix of propensities. Matrix $\mathbf{A}$ is a zero column sum (ZCS) square matrix, as $\mathbf{A}(\mathbf{x},\mathbf{x}) = -\sum_{\mathbf{x}'\neq\mathbf{x}} \mathbf{A}(\mathbf{x}',\mathbf{x})$.

$$\frac{d\mathbf{P}(\mathbf{x},t)}{dt} = \mathbf{A}\mathbf{P}(\mathbf{x},t) \tag{8}$$

Thus, in order to approximate the stationary probability distribution across all microstates, $\mathbf{P_s}(\mathbf{x})$, one can just solve (8) at equilibrium by finding the null space of $\mathbf{A}$, which is unique as this process is irreducible (since the associated graph is strongly connected [21]) and then normalising so that the sum of probabilities of the states adds up to one. We perform this calculation for comparison purposes, but our

aim is to infer features of the stationary distribution directly from the propensities.

B. Directed spanning trees, the Markov chain tree theorem and its consequences

Before presenting the discrete nullcline construct, we first recall the notion of rooted directed spanning trees (also mentioned as arborescences in literature).

Let $G = (V, E, w)$ be a weighted strongly connected directed graph, where $w : E \to \mathbb{R}$ is a weight function defined on its edges. A directed spanning tree rooted at $r \in V$ with orientation from the leaves to the root (i.e. the root vertex is in fact a sink) is a subgraph Q of G such that the undirected version of Q is a tree, while there is a directed path from all vertices in V to the root r [26]. This means that the outdegree (the number of edges directed away from a vertex) of all vertices in Q is equal to 1, whereas the outdegree of r is equal to 0 [11].

From (9), one can see that the null space of $\mathbf{A}$ can be calculated by taking any one column of the adjoint matrix, as it is known that if A is a zero column sum (ZCS) matrix, then adj($\mathbf{A}$) has identical columns [5].

$$(adj(\mathbf{A}))\mathbf{A} = \mathbf{A}(adj(\mathbf{A})) = (\det \mathbf{A})I = 0 \tag{9}$$

From here, moving to the well-known Markov Chain Tree Theorem for $\mathbf{A}$ (an $n \times n$ matrix), presented in Theorem III.1, is natural. We can observe that the elements $a_{j,i}$ of $\mathbf{A}$ correspond to the elements $w_{i,j}$ of a strongly connected directed graph, where $w_{i,j}$ represents the weight of the edge directed from vertex i to vertex j. The weight $W(T)$ of a directed spanning tree T is given by $W(T) = \prod_{edge\, i \to j\, in\, T} w_{i,j} = \prod_{edge\, i \to j\, in\, T} a_{j,i}$.

Theorem III.1. *The i^{th} diagonal of $adj(\mathbf{A})$ is $(-1)^{n-1}$ times the sum of the weights over all directed spanning trees (arborescences) with sink i. [5], [2].*

The first consequence of this theorem is that the stationary probability of every microstate is proportional to the sum of all the directed spanning trees rooted (sinked) on the microstate, as mentioned several times in literature dealing with non-equilibrium dynamics [1], [8]. The second consequence comes from the way the directed spanning trees are formed. As the outdegree of all vertices but the root needs to be equal to one, there can be no directed spanning tree which includes both directions of the same edge (i.e. if the edge $i \to j$ belongs to the directed spanning tree, then the edge $j \to i$ does not).

The third consequence is indirect, yet is critical for constructing a graphical heuristic tool to infer the formation of the stationary probability distribution. For graphs that are balanced (i.e. for each vertex the number of inward edges equals the number of outward edges), such as the one obtained in this genetic toggle switch example, the number of directed spanning trees that can be formed given a particular vertex as the root is constant [24]. Therefore the stationary probability of each microstate is also proportional to the mean weight of the rooted directed spanning trees . This is particularly important, as now we can consider the expected weight of a random directed spanning tree T that can be formed given a distinguished vertex $r = j$.

$$P_s(j) \propto \mathbb{E}(W(T)|root = j) \tag{10}$$

Therefore, if the aim is to infer which roots will have large stationary probabilities, heuristically we need to search for the possible roots that are located in such positions in the graph that would allow the most beneficial directions for each edge to be consistently preferred in their corresponding random directed spanning tree.

C. Discrete 'nullcline' construct proposed

It is evident that in the discrete Markov process setting, the classical notion of nullclines is not applicable, as the ODEs do not capture any effects coming from the 'discreteness' of the system. In the graph formulation, traditional nullclines calculate the difference between the 'birth' and 'death' jump given a particular node, i.e. $f_d = w_{i,i+1} - w_{i,i-1}$ [21] when the birth and death jumps considered occur from node i to nodes $i+1$ and $i-1$ respectively . This, however, does not generalise well with the graph representation coming from the Markov Chain Tree Theorem, especially at the grid boundaries. One can clearly see that at the grid boundaries, f_d in the direction orthogonal to the boundary will always be positive, suggesting that a 'birth' jump is the most probable operation to take place, no matter how strong the propensity of the 'death' jump towards the grid boundary is. The reason for this problem is that the calculation in discrete space depends on two edges, therefore the calculation is not well-defined at the boundaries, as there is no second edge to perform the calculation.
Clearly, a more appropriate calculation, given the fact that a directed spanning tree cannot include both directions of the same edge, would be $f_s = \log\left(\frac{w_{i,i+1}}{w_{i+1,i}}\right)$, taking into consideration the birth jump from node i to node $i+1$ and the death jump from node $i+1$ to node i instead. This means that the sign of f_s provides information about the preferential (largest) transition direction for each edge. It is important, however, to also note the f_s does not just provide a preferential direction, but it is in itself a quantitative measure of the strength of preference of a particular direction. This is particularly important in asymmetric examples, as we will see later.

Furthermore, note that in the 1-D case as well as in higher dimensional cases where detailed balance is satisfied, knowing the f_s value for each edge is sufficient to calculate accurately the entire stationary probability distribution. This is a direct consequence of the definition of detailed balance, which means that for all nodes (vertices) i,j [8],

$$\frac{w_{i,j}}{w_{j,i}} = \frac{P_s(j)}{P_s(i)} \tag{11}$$

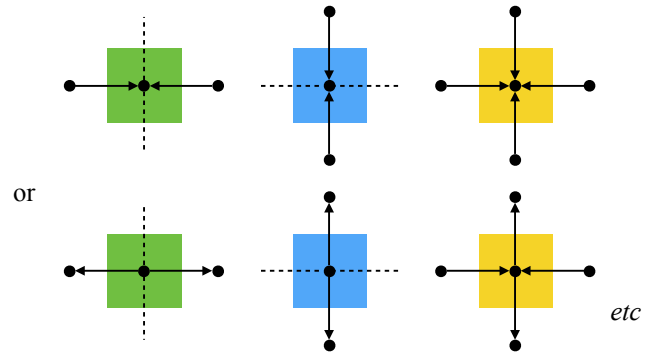

Fig. 1. Illustration of discrete 'nullcline' visualisation procedure. The direction of the arrows represent the direction of the net propensity $\left(f_s = \log\left(\frac{w_{i,i+1}}{w_{i+1,i}}\right)\right)$. The green squares illustrate the net horizontal propensity-reversal nodes, blue squares the net vertical propensity-reversal nodes and yellow squares both net vertical and net horizontal propensity-reversal nodes. Net propensity-reversals take place when the sign of the net propensity changes (i.e.from positive to zero or negative, zero to positive or negative and negative to zero or positive)

It is not a coincidence that in thermodynamics literature, where detailed balance is usually assumed, f_s is used to calculate the local energy difference [20].

Furthermore, this calculation now involves only one edge every time, thus it is well-defined near the grid boundaries as well.

From now on, f_s is to be called the 'net propensity' of each edge. This will be calculated by moving either across the x-axis (horizontal net propensity) or across the y-axis (vertical net propensity).

The aim is to find when the direction of either the net horizontal or the net vertical propensity reverses (i.e. their sign changes from positive to zero or negative, zero to positive or negative and negative to zero or positive). In this way, a discrete 'nullcline' analogue is created.

The procedure of creating visualised 'nullclines' can be done as follows:

- Let $\alpha((p,q),(r,s)), p,q,r,s \in \mathbb{N}_0$ represent the propensity from state (p,q) to state (r,s) i.e. $\frac{dP_{r,s}}{dt} = \alpha((p,q),(r,s))P_{pq} + \ldots$
- If $x > 0$ and $\text{sign}\left(\log\frac{\alpha((x-1,y),(x,y))}{\alpha((x,y),(x-1,y))}\right) \neq \text{sign}\left(\log\frac{\alpha((x,y),(x+1,y))}{\alpha((x+1,y),(x,y))}\right)$ then there is a horizontal net propensity reversal. For visualisation purposes, the square associated with state (x,y) is coloured green.
- If $y > 0$ and $\text{sign}\left(\log\frac{\alpha((x,y-1),(x,y))}{\alpha((x,y),(x,y-1))}\right) \neq \text{sign}\left(\log\frac{\alpha((x,y),(x,y+1))}{\alpha((x,y+1),(x,y))}\right)$ then there is a vertical net propensity reversal. For visualisation purposes, the square associated with state (x,y) is coloured blue.
- If both conditions are satisfied then there is both a horizontal and a vertical net propensity reversal. For visualisation purposes, the square associated with state (x,y) is coloured yellow.

Summarising, net horizontal propensity-reversal nodes are colored green, blue squares illustrate net vertical propensity-reversal nodes and yellow squares represent both net vertical and net horizontal propensity-reversal. Note that it is not possible for a square at the vertical boundary ($x = 0$) to be colored green (or yellow therefore). Similarly it is not possible for a square at the horizontal boundary ($y = 0$) to be colored blue (or yellow). This visualisation procedure is illustrated in Fig.1.

This 'nullcline-like' construct should not be confused with explanatory stochastic 'nullclines' explanations utilising already calculated stationary probability distributions either directly or by Monte Carlo simulations, as in [15], as the construct presented here just utilises the transition rates (propensities) coming directly from the definition of the system. There is no requirement to calculate the steady state solution first. This graphical 'nullcline-like' construction is aimed to allow a very quick, without calculations, inference of the stationary probability distribution as well as provide an insight for the appearance of unexpected probability modes in the stationary probability distribution.

D. Applying the discrete nullclines to the genetic toggle switch example

As shown in Fig. 2, decreasing the equilibrium size $\bar{x} = \bar{y}$, the normalised by the equilibrium fixed point (1,1) varies from being the least dominant mode in the stationary probability distribution to a mode of almost equal probability with the initial two dominant modes, while other modes are appearing as well. The stationary probability distribution of the coarser discretised system (right) can also be used to explain trimodality as an effect of small numbers as this is experimentally observed in [15].

The discretisation observed, inversely proportional to the equilibrium size, has an immediate effect on the discrete 'nullcline' structure of the system, as illustrated in Fig. 2 (bottom). Firstly note that the discrete 'nullclines' when the equilibrium size is large (thus the discretisation is very fine) resemble the deterministic nullclines obtained using Ordinary Differential Equations [7]. Secondly and most importantly, note that the first two discrete 'nullclines' of Fig. 2 are different to the third discrete 'nullclines' diagram as well as to the 'nullclines' of Fig. 3. In the latter two cases we observe a boundary 'nullcline' gap formation, dotted in the figures in red. For the horizontal boundary, for instance, a 'nullcline' gap is formed when the first net horizontal propensity reversal node at the horizontal boundary (coloured green) is to the right of all net vertical propensity reversal nodes (coloured blue or yellow). The exact definition is provided below.

Let the $x-$ and $y-$coordinates of each net horizontal propensity reversal node i be (h_x^i, h_y^i) and belong to set H. Let the $x-$ and $y-$coordinates of each net vertical propensity reversal node j be (v_x^j, v_y^j) and belong to set V. Let the largest x-coordinate component found in the elements of set V be v_x^{max} and the largest y-coordinate component found in the elements of set H be h_y^{max}. Let $h_{x,0}^{min}$ be the minimum x-coordinate

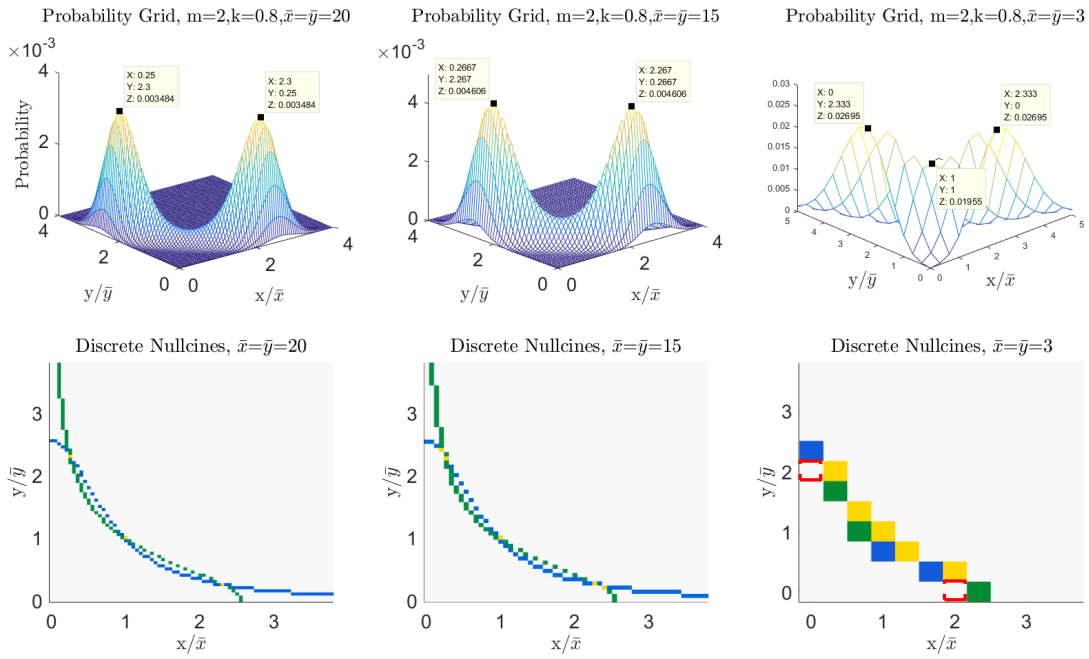

Fig. 2. The stationary probability distributions (top) with the corresponding discrete 'nullclines' (bottom) in the case of cooperative binding (m=2, k=0.8). By decreasing $\bar{\mathbf{x}} = \bar{\mathbf{y}}$ (20 to 15 to 3), the normalised by the equilibrium fixed point (1,1) varies from being the least dominant mode in the stationary probability distribution to a mode of almost equal probability with the initial two dominant modes. Note that there is no boundary 'nullcline' gap formation (like the ones dotted in red) in the first two cases ($\bar{\mathbf{x}} = \bar{\mathbf{y}} = \mathbf{20}$ and $\bar{\mathbf{x}} = \bar{\mathbf{y}} = \mathbf{15}$), and that the initial two dominant modes are not found exactly on the boundaries of the grid in contrast with the results in Fig.3. The stationary probability distribution when the equilibrium size is small (and discretisation is coarse) (right) can be used to explain the trimodality observed experimentally in [15].

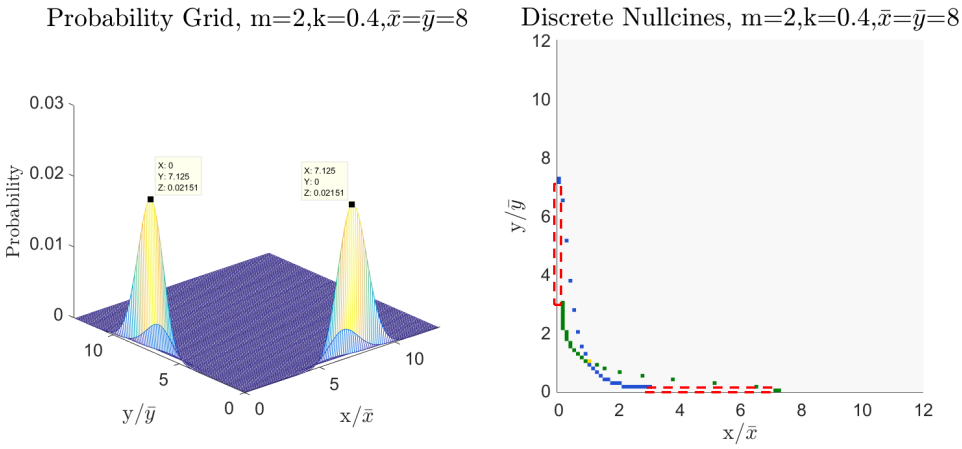

Fig. 3. m=2, k=0.4, $\bar{\mathbf{x}} = \bar{\mathbf{y}} = \mathbf{8}$. The net horizontal and net vertical propensity-reversal nodes form a 'nullcline' gap on each boundary which is dotted in red, where the orthogonal to the boundary net propensities are pointing towards the boundary.

component of the elements $(h_x^i, 0)$ of set H and $v_{0,y}^{min}$ be the minimum y-coordinate component of the elements $(0, v_y)$ of set V. Then,

Definition III.2. A horizontal boundary 'nullcline' gap is defined to be formed when $h_{x,0}^{min} > v_x^{max}$. If that is true, then the size of the gap is equal to $h_{x,0}^{min} - v_x^{max}$. Similarly, a vertical boundary 'nullcline' gap is defined to be formed when $v_{0,y}^{min} > h_y^{max}$. If that is true, then the size of the gap is equal to $v_{0,y}^{min} - h_y^{max}$.

This essentially means that the preferential direction of the orthogonal to the boundary edge is towards the boundary (i.e. towards zero), whereas the preferential direction of the parallel to the boundary edge is towards further growth. This can be interpreted by saying that it is preferential for one

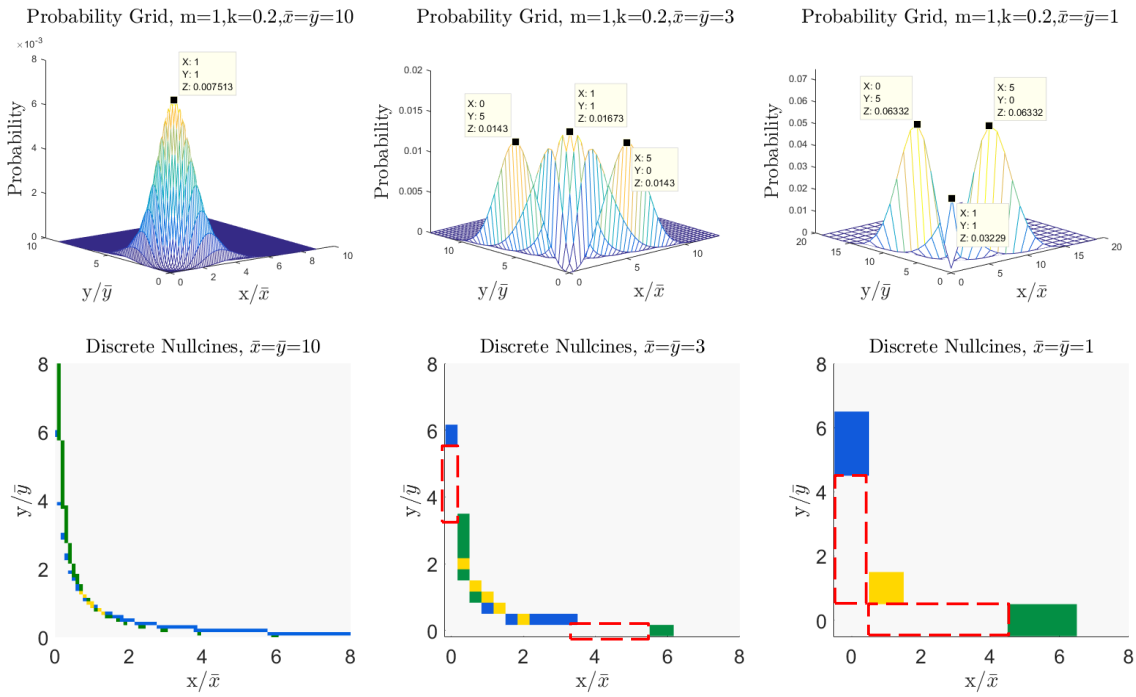

Fig. 4. The stationary distributions (top) with the corresponding discrete 'nullclines' (bottom) for the non-cooperative binding case (m=1). By decreasing $\bar{\mathbf{x}} = \bar{\mathbf{y}}$, the normalised by the equilbrium fixed point (1,1) (which is always coloured yellow as it is both a net vertical and a net horizontal propensity-reversal node) varies from being the dominant mode in the stationary probability distribution to the least dominant mode, while two dominant modes appear on the boundaries. At the same time boundary 'nullcline' gaps are formed (dotted in red) in both the horizontal and the vertical boundaries.

species to completely vanish, while it is preferential for the other species to continue growing.

Fig. 3 greatly resembles the examples in literature where the genetic toggle switch with no cooperative binding exhibits bimodality [14].

For that reason, the same analysis was performed for the genetic toggle switch with no cooperative binding (m=1), the results of which are shown in Fig.4. When discretisation is very fine (left), the discrete 'nullclines' resemble what we get with deterministic nullclines, accompanied with monomodality in the stationary distribution. Yet, as the equilibrium size becomes smaller and therefore the discretisation becomes coarser, the discrete 'nullclines' reveal the gap on the grid boundaries as that observed in Fig. 3, explaining the movement from monomodality to an intermediate multimodality and finally to essentially bimodality with the two modes always found on the boundaries, as in Fig. 3.
These results show that the discrete 'nullclines' proposed can capture the effects of the changes in both the equilibrium size and k, associated with the inverse of the repression strength, and provide the insight that the mechanism providing bimodality in the non-cooperative binding case can, in certain cases, be the same mechanism providing bimodality in the cooperative binding case (e.g. as in Fig. 3).

IV. The Comparison with Numerical Methods Illustrates that the Heuristic Method Provides Upper-Bound Estimates

Clearly, the discrete 'nullclines' constructed can provide a good starting point for inference of potential stochastic effects, prior to any calculations. In this section we aim to compare the value of k, associated with the inverse of the repression strength, obtained through the heuristic nullcline procedure with the minimum numerically-found value of k, which guarantees that the corresponding to the equilibrium point, $(\bar{x},\bar{x})$, $\bar{x}=\bar{y}$, node in the associated graph is the global mode.

Proposition IV.1 provides the necessary and sufficient condition relating the equilibrium size $\bar{x}(=\bar{y})$ and the parameter associated with the inverse of the repression strength, k, for the discrete 'nullcline' boundary gap to be formed.

Proposition IV.1. *Consider the symmetric genetic toggle switch system presented in* (1) *with* $\beta = \frac{k^m}{k^m+1}$, $\bar{x}=\bar{y}\geq 1$ *and* $k>0$. *Horizontal and vertical boundary 'nullcline' gaps are formed, as defined in Definition III.2, if and only if* $\lceil \frac{k^m+1}{k^m}\bar{x}-1\rceil > \lfloor \sqrt[m]{(k^m+1)\bar{x}^{m+1}-k^m\bar{x}^m}\rfloor$

Proof: At point $(0,0)$ the net vertical and the net horizontal propensities are both equal to $f_s = \log\left(\frac{\bar{x}(k^m+1)}{k^m}\right)$. For $\bar{x}\geq 1$ and $k>0$, $f_s>0$. Looking at the horizontal boundary, the horizontal net propensity is given by $f_{sH} = \log\left(\frac{\bar{x}(k^m+1)}{(x+1)k^m}\right)$, whereas the vertical net propensity is given

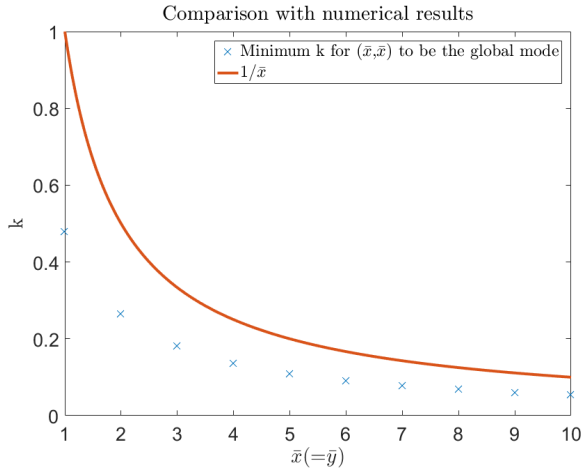

Fig. 5. In the regime of small numbers and non-cooperativity ($m=1$), we compare, for different equilibrium solutions, the numerically-found minimum k for $(\bar{x},\bar{x})$, $\bar{x}=\bar{y}$, to be the global mode (i.e. the node with unique maximum stationary probability) against the sufficient ($k<1/\bar{x}$) condition obtained for the formation of boundary 'nullcline' gaps.

by $f_{sV}=\log\left(\frac{\bar{y}(k^m+1)}{k^m+\left(\frac{\bar{x}}{\bar{x}}\right)^m}\right)$. It is easily seen that as we increase x both terms will monotonically decrease and ultimately become negative. For a fixed x, x_0, the vertical net propensities as y is increased are also monotonically decreasing as can be seen: $f_{sV}^{y}=\log\left(\frac{\bar{y}(k^m+1)}{(y+1)\left(k^m+\left(\frac{x_0}{\bar{x}}\right)^m\right)}\right)$. Therefore we only need to find the points where the change of sign occurs at the boundary. Balancing the horizontal propensities of the edge on the right of $(x_H,0)$ for $\bar{x}=\bar{y}$,

$$\frac{k^m}{k^m+1}\frac{x_H+1}{\bar{x}}=1\Rightarrow x_H=\frac{k^m+1}{k^m}\bar{x}-1$$

Balancing the vertical propensities of the edge on the top of $(x_V,0)$,

$$\frac{k^m}{k^m+1}\frac{1}{\bar{x}}=\frac{k^m}{k^m+\left(\frac{x_V}{\bar{x}}\right)^m}$$
$$\Rightarrow x_V=\sqrt[m]{(k^m+1)\,\bar{x}^{m+1}-k^m\bar{x}^m}$$

Thus

$$\lceil x_H\rceil>\lfloor x_V\rfloor\Leftrightarrow\left\lceil\frac{k^m+1}{k^m}\bar{x}-1\right\rceil>\left\lfloor\sqrt[m]{(k^m+1)\,\bar{x}^{m+1}-k^m\bar{x}^m}\right\rfloor$$

Since $h_{x,0}^{min}=\lceil x_H\rceil$ and $v_x^{max}=\lfloor x_V\rfloor$, it follows that there exists a horizontal boundary 'nullcline' gap (see Definition III.2) under the same condition. The same calculation applies to the vertical boundary due to the symmetry of the problem. □

A sufficient condition for boundary 'nullcline' gap formations is the one presented in Proposition IV.1, yet without taking the floor and ceiling operations into account. For non-cooperative binding ($m=1$), $\bar{x}=\bar{y}\geq 1$, and $k>0$, this sufficient condition simply becomes $k<1/\bar{x}\leq 1$.
Figure 5 illustrates that, in the regime of small numbers, the sufficient value of k for boundary 'nullcline' gap formations, is an upper-bound estimate of the numerically-found minimum k for the equilibrium point $(\bar{x},\bar{y})$, $\bar{x}=\bar{y}$, to be the global mode when $m=1$. The reason the latter is calculated for integers only, is that an integer is required for the equilibrium point in the deterministic domain to coincide exactly with a vertex (microstate) in the corresponding graph depicting the Markov process.

Although k in Fig. 5 can be found numerically directly by calculating the null space of matrix $\mathbf{A}$ for each k, we use a formulation of ours proved in [19], extending a result by Karim et al [13]. In our formulation $\mathbf{A}'q=b$, where $\mathbf{A}'$ is the principal submatrix of $\mathbf{A}$ after the removal of the row and of the column corresponding to the equilibrium microstate j without loss of generality. b is the j^{th} column of $\mathbf{A}$ with element j deleted. $q=\left[q_1,q_2,q_3,...,q_{j-1},q_{j+1},q_{j+2},...,q_n\right]^T$, $q_k=\left[\frac{P_s(k)}{P_s(j)}\right]$, represents the vector of ratios of stationary probabilities of all the nodes compared to the stationary probability of the microstate j. Then the microstate j is the unique global mode if and only if $\|q\|_\infty<1$. Therefore another way to investigate this problem numerically is by investigating $\|q\|_\infty$ in the parameter space of $\bar{x}$ and k.

V. The discrete 'nullcline' construct can also be used in the asymmetric case

Even though up to now we only considered the symmetric case of the toggle switch, as this is the one most commonly investigated in literature [16], [14], we would like to emphasize that the discrete 'nullclines' we propose can be used effectively in asymmetric cases as well. For example, (12) increases both the 'birth' as well as the 'death' rates associated to species x, while leaving the corresponding rates for y equal to the ones shown in (1).

$$\begin{aligned} x &\xrightarrow{\frac{(1.2k)^m\bar{x}}{(1.2k)^m+\left(\frac{y}{\bar{y}}\right)^m}} x+1, x\xrightarrow{1.3\beta x}x-1\\ y &\xrightarrow{\frac{k^m\bar{y}}{k^m+\left(\frac{x}{\bar{x}}\right)^m}} y+1, y\xrightarrow{\beta y}y-1 \end{aligned} \tag{12}$$

In Fig. 6 we can see that the boundary modes in the stationary probability distribution can be predicted from the boundary gaps of the corresponding discrete 'nullclines'. As this case is asymmetric however, we need to make a further prediction regarding which of the two boundary gaps will produce the largest mode. To do so, we can use the value of the net propensities (i.e. the logarithm of the ratio of the weights of the two directions of each edge) of the edges orthogonal to the boundary gaps. It is observed that in the horizontal boundary, the vertical net propensity is less negative than the horizontal net propensity at the vertical boundary, while the size of the 'nullcline' boundary gap is also smaller. Therefore, we expect to have the largest mode on the vertical boundary, which is exactly what we observe.

VI. Conclusions

We have proposed a new discrete 'nullcline' construct, inspired by the Markov chain tree theorem, aimed to be

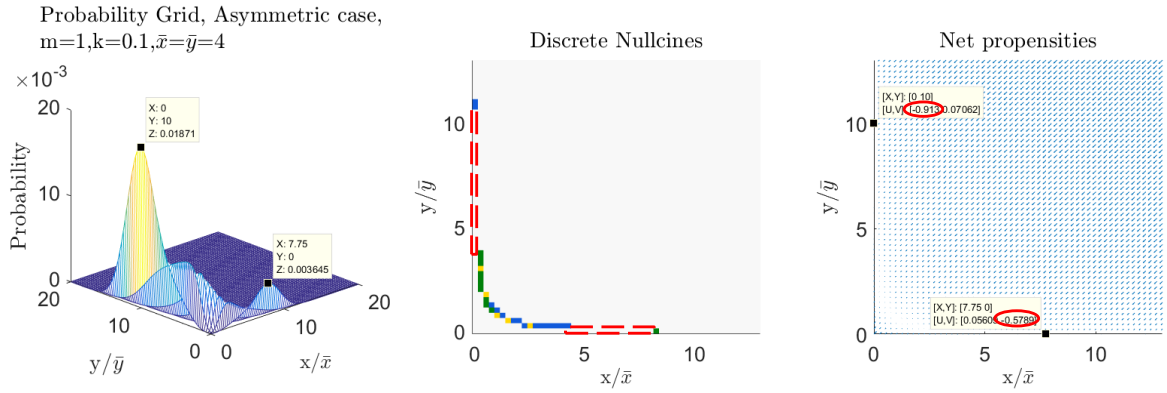

Fig. 6. The discrete 'nullclines' can be used to provide predictions for the stationary probability distributions in the asymmetric genetic toggle switch example as well. For the asymmetric case presented in (12) with $m = 1$, $k = 0.1$, $\bar{x} = \bar{y} = 4$, we also need to make a further prediction regarding which of the two boundary 'nullcline' gaps will produce the largest mode. To do so, we can use the value of the net propensities of the edges orthogonal to the boundary gaps. It is observed that in the horizontal boundary, the vertical net propensity is less negative than the horizontal net propensity at the vertical boundary. Therefore, we expect to have the largest mode on the vertical boundary, which is exactly what we observe.

used as a heuristic graphical tool for investigating stochastic phenomena, requiring minimum calcluations. Its effectiveness was investigated through the genetic toggle switch example, where it was illustrated that it is effective in finding parameter regimes where different stochastic phenomena are to be expected as well as providing good inference of the stationary probability distributions to be expected both in the symmetric and asymmetric cases. Unlike other constructs [15], its aim is not to be explanatory but predictive, thus requiring no previous calculation of the steady-state distribution either through direct means [17], [21] or through Monte Carlo Simulations [15].

References

1. Tobias Ahsendorf, Felix Wong, Roland Eils, and Jeremy Gunawardena. A framework for modelling gene regulation which accommodates non-equilibrium mechanisms. *BMC biology*, 12(1):102, 2014.
2. Venkat Anantharam and Pantelis Tsoucas. A proof of the markov chain tree theorem. *Statistics & Probability Letters*, 8(2):189–192, 1989.
3. William Bialek and Sima Setayeshgar. Cooperativity, sensitivity, and noise in biochemical signaling. *Physical Review Letters*, 100(25):258101, 2008.
4. Tommaso Biancalani and Michael Assaf. Genetic toggle switch in the absence of cooperative binding: Exact results. *Physical review letters*, 115(20):208101, 2015.
5. Philip Feinsilver. Matrices with zero row sums, tree theorems and a markov chain on trees. *Probability on Algebraic and Geometric Structures*, 668:67, 2016.
6. Harold N Gabow, Zvi Galil, Thomas Spencer, and Robert E Tarjan. Efficient algorithms for finding minimum spanning trees in undirected and directed graphs. *Combinatorica*, 6(2):109–122, 1986.
7. Timothy S Gardner, Charles R Cantor, and James J Collins. Construction of a genetic toggle switch in escherichia coli. *Nature*, 403(6767):339–342, 2000.
8. Bernard Gaveau and LS Schulman. Master equation based formulation of nonequilibrium statistical mechanics. *Journal of Mathematical Physics*, 37(8):3897–3932, 1996.
9. Daniel T Gillespie. The chemical langevin equation. *The Journal of Chemical Physics*, 113(1):297–306, 2000.
10. Gary Gordon and Elizabeth McMahon. A greedoid polynomial which distinguishes rooted arborescences. *Proceedings of the American Mathematical Society*, 107(2):287–298, 1989.
11. Ronald Gould. *Graph theory*. Dover, 2012.
12. Sanjiv Kapoor and H Ramesh. Algorithms for generating all spanning trees of undirected, directed and weighted graphs. In *Workshop on Algorithms and Data Structures*, pages 461–472. Springer, 1991.
13. Shahriar Karim, Gregery T Buzzard, and David M Umulis. Efficient calculation of steady state probability distribution for stochastic biochemical reaction network. *BMC genomics*, 13(Suppl 6):S10, 2012.
14. Azi Lipshtat, Adiel Loinger, Nathalie Q Balaban, and Ofer Biham. Genetic toggle switch without cooperative binding. *Physical review letters*, 96(18):188101, 2006.
15. Rui Ma, Jichao Wang, Zhonghuai Hou, and Haiyan Liu. Small-number effects: a third stable state in a genetic bistable toggle switch. *Physical review letters*, 109(24):248107, 2012.
16. Marco Maggioni, Tanya Berger-Wolf, and Jie Liang. Gpu-based steady-state solution of the chemical master equation. In *Parallel and Distributed Processing Symposium Workshops & PhD Forum (IPDPSW), 2013 IEEE 27th International*, pages 579–588. IEEE, 2013.
17. Brian Munsky and Mustafa Khammash. The finite state projection algorithm for the solution of the chemical master equation. *The Journal of chemical physics*, 124(4):044104, 2006.
18. Randip Pal. Relationships between models of genetic regulatory networks with emphasis on discrete state stochastic models. In *Emerging Research in the Analysis and Modeling of Gene Regulatory Networks*, pages 52–79. IGI Global, 2016.
19. Andreas Petrides and Glenn Vinnicombe. Enzyme sequestration by the substrate and the consequent drive towards bistability/bimodality: An analysis in the deterministic and stochastic domains. *Manuscript submitted for publication*, 2017.
20. Hong Qian. Thermodynamics of markov processes with non-extensive entropy and free energy. *arXiv preprint arXiv:1005.1251*, 2010.
21. Daniel Schultz, Aleksandra M Walczak, José N Onuchic, and Peter G Wolynes. Extinction and resurrection in gene networks. *Proceedings of the National Academy of Sciences*, 105(49):19165–19170, 2008.
22. Steven H Strogatz. *Nonlinear dynamics and chaos: with applications to physics, biology, chemistry, and engineering*. Westview press, 2014.
23. Tsz-Leung To and Narendra Maheshri. Noise can induce bimodality in positive transcriptional feedback loops without bistability. *Science*, 327(5969):1142–1145, 2010.
24. William Thomas Tutte. *Graph theory as I have known it*. OUP Oxford, 1998.
25. N Gr van Kampen. Stochastic processes in physics and chemistry, 1995.
26. Lecturer Uri Zwick. Lecture notes on analysis of algorithms: Directed minimum spanning trees, 2013.